Int J Adv Manuf Technol (2016) 85:2761–2771
DOI 10.1007/s00170-015-8135-6

ORIGINAL ARTICLE

Application of sliced inverse regression with fuzzy clustering for thermal error modeling of CNC machine tool

Ting Zhang[1,2] · **Wenhua Ye**[2] · **Yicai Shan**[3]

Received: 24 July 2015 / Accepted: 12 November 2015 / Published online: 24 November 2015

Abstract Thermal error significantly influences the accuracy of CNC machine tool. A high-performance compensation system depends upon the accuracy and robustness of the model and appropriate model inputs of temperatures. In this paper, fuzzy clustering is conducted in temperature classification. Based upon an evaluation model, an optimal temperature classification can be found. The representative temperatures from each group construct temperature candidates. Then, a sliced inverse regression (SIR) model is introduced in thermal error modeling, which can change the problem of high-dimensional forward regression into several one-dimensional regression and meanwhile further eliminate the coupling among temperatures candidates. To evaluate the performance of SIR model, measuring experiment was carried out on a horizontal machining center for temperature and thermal error information under two experimental conditions. The proposed classification method was used to classify 29 temperature variables into five groups. A SIR model was built upon the five temperature candidates. Meanwhile, stepwise regression (SR) theory is also conducted for temperature variable selection and thermal error modeling. Comparison shows that both of the two models have high fitting accuracy, while the SIR model is more excellent in robustness than the SR model. Finally, a compensation system was developed. Compensation experiment shows that the SIR model is practical and effective, which can reduce the axial thermal error from 43 to 7 μm.

Keywords Thermal error · Sliced inverse regression · Machine tool · Error compensation

✉ Ting Zhang
tingnjit@163.com

[1] School of Mechanical Engineering, Nanjing Institute of Technology, Nanjing 211167, People's Republic of China

[2] College of Mechanical and Electrical Engineering, Nanjing University of Aeronautics and Astronautics, Nanjing 210016, People's Republic of China

[3] School of Mechanical and Electrical Engineering, Nanjing College of Information Technology, Nanjing 210046, People's Republic of China

1 Introduction

Research shows that machining accuracy closely relates to geometric and kinematic accuracies of machine structure, deformation induced by heat and cutting force, tool wear, servo control error, etc. In precision machine tool, thermal error is the main reason for the relative displacement between the tool and the workpiece. According to various publications [1], thermal error accounts for 45 to70% of the total machining error. To improve the machining accuracy, thermal error compensation is a cost-effective approach. With the variation of environment, working cycle, and working parameters, the temperature field of machine tool becomes nonuniform. Thermal error shows the characteristics of nonlinearity and time-dependent nature. Hence, accurate model of thermal error is hard to be built.

1.1 Thermal error modeling method

There are two general schools of thought in thermal error compensation [2]. The first method is numerical analysis, such as finite element method (FEM) and finite difference method (FDM). Mian et al. [3] proposed a novel off-line thermal error modeling method using FEM. The method significantly reduced the machine downtime required to establish the thermal

response. Mayr et al. [4] firstly used FDM to analyze the transient and steady temperature, then applied FEM to obtain thermal errors. However, the perfect boundary conditions and the accurate characteristics of heat transfer are difficult to obtain when building the numerical simulation model.

The second method is empirical modeling which maps the relation between temperature and thermal error. Many theories have been introduced in thermal error modeling, such as regression theory [5–7], artificial neural networks (ANNs) [8], grey system theory [9], Bayesian theory [10], fuzzy logic [11], and support vector machines (SVMs) [12, 13].

With simple structure and convenient application, regression analysis is the most common used method in thermal error modeling. Wu et al. [5] built a multiple regression (MR) model of positioning error and reduced the axial positioning error from 20 to 3 μm. Han et al. [6] and Vyroubal [7] applied MR into thermal error modeling, respectively, and proved its effectiveness through experiments. Although MR model can provide reasonable results for a given working condition, the model might not fit for the other working conditions as the thermal displacement and temperature usually change with the variation of machining process and the environment.

ANN is another familiar theory in thermal error modeling which is able to improve the model robustness. Chen et al. [8] used ANN in the real-time prediction of thermal error and proved the model effectiveness on a machining center. The biggest challenge in ANN is determining the hidden layer of ANN model. In recent years, many algorithms (such as particle swarm optimization algorithm, ant colony algorithm, and genetic algorithm) have been combined with ANN for better convergence speed and prediction accuracy [14–16].

Li et.al. [9] built thermal error models with total data grey model (GM)(1,1), new information GM(1,1), and metabolic GM(1,1). The modeling results showed that the prediction precision of the metabolic GM(1,1) was 7.2 and 15.46 % higher than the other two models. Since the accumulated generating operation (AGO) uses the accumulation of previous data to reduce the randomness of the data, the thermal error model can describe the long-term trend of the data. Unfortunately, some short-term dynamics of the system might be lost due to AGO. Therefore, the model obtained under one particular operation condition might not be robust under other operation conditions.

Yao et al. [10] established a Bayesian network (BN) model for thermal error and improved the accuracy by approximately 80 %. The contrasted result showed that the BN method was better than the least squares (LS) model in terms of modeling estimation accuracy. The Bayesian network model has good dynamic performance. But, under the high sampling frequency, the number of network notes increases and the system becomes more complicated; the network training is a big difficulty.

Korea scholars advanced a fuzzy logic strategy for thermal error modeling, which had good robustness without precise mathematical model [11]. However, the heavy dependence on experience limits its application in thermal error modeling.

R Ramesh et al. [12] introduced SVM and ANN in thermal error modeling. They found that the SVM model was much faster, easier to develop, and required fewer data. Besides, Miao et al. [13] built thermal error model with SVM and pointed out that the SVM model had high fitting accuracy, good retaining ability, and strong robustness. Since the solution of support vectors is based upon quadratic programming, the method is difficult to use for great sample data.

To take full advantages of different modeling theories, scholars have advanced many hybrid methods for thermal error modeling, such as Bayesian network-support vector machine model [17], grey neural network model [18], and adaptive neuro-fuzzy inference system (ANFIS) prediction model [2].

1.2 Optimization of model inputs

In empirical modeling, temperatures are often used as inputs. Intuitively, a large number of temperature sensors can accurately describe the temperature distribution of CNC machine tool. However, too many sensors might increase the workload and the cost in thermal error compensation, as well as influence the normal operation of CNC machine tool. Besides, excessive sensors might reduce measurement precision since there is correlation between signal and noise. Therefore, the optimization of temperature sensors is necessary before modeling.

Apart from engineering judgment, finite element analysis and many mathematical theories have been used in selecting temperature sensors, such as correlation analysis, stepwise regression (SR), fuzzy c-means clustering, and grey relational analysis [2, 19]. Based on thermal error sensitivity technology, Zhao et.al [20] proposed a selection principle of thermal key points after simulating the temperature field and thermal errors using finite element analysis. However, the difficulty in determining the boundary conditions limits the application of the method. The correlation analyses are usually conducted to calculate the correlation coefficients, which can describe the relevance between temperatures and the relations between temperature and thermal error [15]. Chen et al. [8] screened out independent temperature variables based on experience and the correlation analysis at first, then applied SR analysis for a second screening. Han et.al [21] applied fuzzy c-means clustering and selected 4 representative temperature variables from 32 temperature variables. Yan et.al. [22] adopted grey relationship analysis in temperature sensor optimization and reduced temperature sensors from 16 to 4. However, these mathematical theories still suffer from different drawbacks. Fuzzy c-means clustering is sensitive to initial value and easily falls into local minimum. In fuzzy c-means clustering analysis, the determination of the optimal cluster

number is a difficult problem. As for correlation analysis and grey relationship analysis, the threshold in temperature classification is usually determined by engineering judgment. So, the scientific basis for temperature classification is not clear. Meanwhile, multicollinearity is often overlooked in grey relationship analysis. In SR, one temperature variable is added or deleted at each step. The effect of combining two or more temperature variables at a time is never considered, which may affect the accuracy of thermal error model [19].

In this paper, an evaluation model is firstly established for optimal temperature classification based on fuzzy clustering. According to the correlation coefficients between temperature variables and thermal error, one of the variables in each temperature group is selected as representative variable. The multiple representative variables chosen from different temperature groups are regarded as temperature candidates. Secondly, a sliced inverse regression (SIR) model is proposed for thermal error prediction. Next, the temperature field and thermal error were measured on a precise horizontal machining center with 29 temperature sensors and 5 displacement sensors. Based upon correlation analysis, five temperature candidates were determined and used as inputs of a SIR model. Comparison was made on the performance of a SIR model and a SR model. Finally, a thermal error compensation systems was developed and compensation experiment was carried out which proved the good prediction accuracy of the SIR model.

2 Temperature classification based on fuzzy clustering

Since there is no firm demarcation in temperatures variables, the temperature classification is somewhat intermediate which can be realized by soft division with the fuzzy set theory. According to the closeness degree and similarity of temperature variables, the fuzzy theory completes the classification through fuzzy similar relation. To verify the efficiency of classification and to obtain an optimal temperature classification, evaluation model is needed [23].

2.1 Calculation of fuzzy equivalence matrix

To describe the relativity of temperature variables, correlation coefficient matrix R is constructed as the following:

$$R = \left(r_{ij}\right)_{p\times p}, \quad 1\le i,j\le p \tag{1}$$

where p is the number of temperature variables. The element r_{ij} is defined as the correlation coefficient of the ith temperature t_i and the jth temperature t_j, which is expressed as

$$r_{ij} = \frac{\sum_{k=1}^{n}\left|t_{ik}-\bar{t}_i\right|\left|t_{jk}-\bar{t}_j\right|}{\sqrt{\sum_{k=1}^{n}\left(t_{ik}-\bar{t}_i\right)^2}\sqrt{\sum_{k=1}^{n}\left(t_{jk}-\bar{t}_j\right)^2}} \tag{2}$$

Here, $\bar{t}_i = \frac{1}{n}\sum_{m=1}^{n} t_{im}$ and $\bar{t}_j = \frac{1}{n}\sum_{m=1}^{n} t_{jm}$. The note n is the sample number in each temperature variable.

According to the maximum-minimum principles, a series of compositional operation is made.

$$R\circ R = R^2, \quad R^2\circ R^2 = R^4, \ldots, \quad R^{2^k}\circ R^{2^k} = R^{2^{k+1}} \tag{3}$$

When k satisfies $R^{2^k} = R^{2^{k+1}}$, fuzzy equivalence matrix $\tilde{R}$ is found, which equals to R^{2^k}.

2.2 Establishment of evaluation model for temperature classification

Under the fuzzy equivalence matrix $\tilde{R}$, the minimum element of $\tilde{R}$ is set as initial threshold $\lambda_{\min}$ and the maximum element as final threshold $\lambda_{\max}$. Then, the threshold increment $\Delta\lambda$ is determined according to the values of $\lambda_{\min}$ and $\lambda_{\max}$.

Suppose threshold value λ can classify all temperature variables into f_λ groups which are $u_1, u_2, \ldots, u_{f_\lambda}$. The ith group u_i has q temperature variables. Each temperature variable sequence in group u_i (i=1,2,…,f_λ) can be expressed as

$$t_k^{(i)} = \left\{t_{k,1}^{(i)}, t_{k,2}^{(i)}, \ldots, t_{k,n}^{(i)}\right\}, \quad k = 1,2,\ldots,q, i = 1,2,\ldots,f_\lambda \tag{4}$$

Define the center of group u_i as $t^{(i)}$ and the center of total temperature variables as $\bar{t}$. Here,

$$t^{(i)} = \frac{1}{q}\sum_{k=1}^{q} t_{k,l}^{(i)}, l = 1,2,\ldots,n \tag{5}$$

$$\bar{t} = \frac{1}{p}\sum_{j=1}^{p} t_{j,l}, l = 1,2,\ldots,n \tag{6}$$

The evaluation model can be described as

$$F = \frac{\sum_{i=1}^{f_\lambda}\left\|t^{(i)}-\bar{t}\right\|^2/(f_\lambda-1)}{\sum_{i=1}^{f_\lambda}\left(\frac{1}{n_i}\sum_{j=1}^{n_i}\left\|t_j^{(i)}-t^{(i)}\right\|^2\right)/(p-f_\lambda)} \tag{7}$$

In formula (7), $\frac{1}{n_i}\sum_{j=1}^{n_i}\left\|t_j^{(i)}-t^{(i)}\right\|^2$ describes the relationship between temperature variables in group u_i. The small value

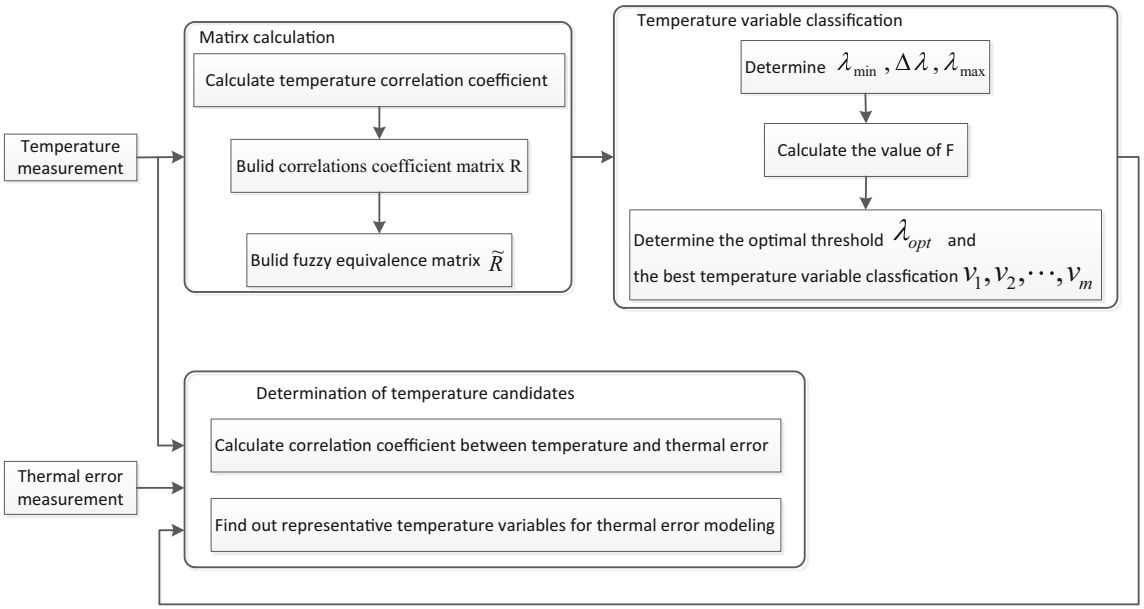

Fig. 1 Process of temperature candidate optimization

means the close relationship. $\left\|t^{(i)}-\bar{t}\right\|^2$ denotes the distance between $t^{(i)}$ and $\bar{t}$. Big value of the evaluation model F means large difference between groups and small distance between temperature variables of each group. Based upon $\lambda_{\min}$, $\lambda_{\max}$, and $\Delta\lambda$, a series of calculation is made using formula (7).

2.3 Determination of temperature candidates

The biggest value of F is corresponding to optimal threshold λ_{opt}. Under λ_{opt}, the best temperature classification $v_1, v_2, \cdots, v_m$ can be found. In group v_i $(i=1,2,\cdots m)$, correlation analysis is made between temperatures and thermal error. The temperature variable which corresponds to the maximum correlation coefficient is regarded as the representative temperature of the group. The m representative temperatures chosen from $v_1, v_2, \cdots, v_m$ are regarded as temperature candidates.

The process of temperature candidate optimization is shown in Fig. 1.

3 Forward regression model of thermal error

In thermal error compensation, regression theory has been widely used for error prediction because of the simple structure and easy implementation. Most thermal error regression models are based on forward regression which has fixed model parameters, such as polynomial regression (PR) model and MR model.

Define the independent variables as X and the dependent variable as y. The number of temperature variables in X is p. The data set T can be described as $T=\{(x_1,y_1),(x_2,y_2),\cdots,(x_n,y_n)\}$, where $x_i \in X \subseteq R^p, y_i \in y \subseteq R^1$.

To build forward regression model, five steps are necessary:

① Determine the relational function $y=f(X)$.
② Restrict the function set F which is composed by $f(X)$.
③ Select a lost function $c(X,y,f)$ to determine the deviation between y_i and $f(x_i)$.
④ Define empirical risk $R_{\text{emp}}=\sum_{i=1}^{n} c(x_i,y_i,f(x_i))$.
⑤ Find out the $f(X)$ which can minimize empirical risk R_{emp} in F.

From the above, we know that the forward regression model is a type of parametric model. Once the parameters are determined on the basis of experimental data, the model form is fixed. In long-term prediction, if the tendency of

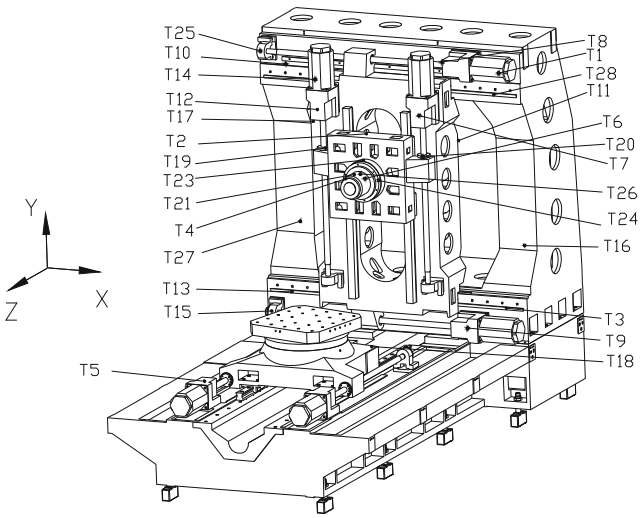

Fig. 2 Machining center and thermocouple location

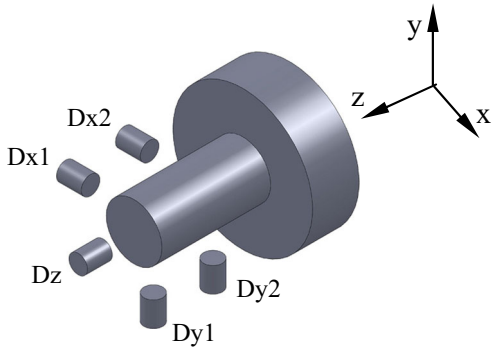

Fig. 3 Distribution of five displacement sensors

independent variable does not agree with the tendency at the beginning of the modeling, the prediction accuracy will decrease. Meanwhile, if the optimized temperature input still has collinearity after thermal key point selection, the model accuracy will be influenced. Therefore, the forward regression model has poor extrapolation capability and low generalization ability.

4 Sliced inverse regression model of thermal error

In forward regression, X is used as input to calculate y. While in inverse regression, regression calculation is made on the basis of y to obtain the component in X. Without nonparametric smoothing, inverse regression changes the problem of high-dimensional forward regression into several one-dimensional regression, which can reduce data dimension.

SIR advanced by Ker-Chau Li in 1991 [24] is a method based on nonparametric inverse regression. Under the assumption of nonlinear model, SIR can reduce the dimension of high-dimensional independent variables without parametric assumption. Besides, under minimum information loss, SIR synthesizes the original variables into principle components, which can avoid information overlap and high correlation, and further optimizes model inputs. With the virtues of wide applicability and easy implementation, SIR has been used in many fields.

Given the dependent variable $y \subseteq R^1$ and independent variable $X \subseteq R^p$, SIR is based on the model

$$y = g(\beta_1 X, \beta_2 X, \cdots, \beta_k X, \varepsilon) \tag{8}$$

where g is an unknown function in space R^{k+1}, $\beta_1, \beta_2, \cdots, \beta_K$ are unknown row vector, and ε is the error with $E[\varepsilon|X]=0$. Under minimum information loss, p-dimensional independent variable X is projected onto k-dimensional subspace $(\beta_1 X, \beta_2 X, \cdots, \beta_k X)^T$ through $\beta_i (i=1,2,\cdots,k)$. When $k<p$, dimension of X is reduced.Any linear combination of $\beta_1, \beta_2, \cdots, \beta_K$ is regarded as an effective dimension reduction (e.d.r.) direction, and the linear space generated by $\beta_1, \beta_2, \cdots, \beta_K$ is e.d.r. space. After the estimation of β_i, methods from nonparametric statistics will be used to calculate unknown function g.In thermal error modeling, we define the thermal error y as $y=[y_1, y_2, \cdots, y_n]$ and temperature variable as $X=[x_1, x_2, \cdots, x_n]$, among which $x_i=[x_{i1}, x_{i2}, \ldots, x_{ip}]^T$ $(i=1, \cdots, n)$. The modeling steps of SIR are as the following:

① Standardization of independent variable

Standardize X by an affine transformation to get a new matrix $\tilde{X} = [\tilde{x}_1, \tilde{x}_2, \cdots, \tilde{x}_n]$, where $\tilde{x}_i = \sum_{xx}^{-1/2}(x_i - \overline{x})$ $(i = 1, 2, \cdots, n)$. $\sum_{xx}$ represents the sample covariance of X, and $\overline{x}$ is the sample mean of X.

② Sorting and slicing of sample data

Sort thermal error y to form a new sequence y_P. Divide range of y_P into H slices, $I_1, I_2, \cdots, I_H$. The proportion of the $y_{Pi} (i=1,2,\cdots,n)$ that falls in slice $I_h (h=1,\cdots,H)$ is defined as $\hat{p}_h$. Here, $\hat{p}_h = (1/n)\sum_{i=1}^{n} \delta_h(y_{Pi})$, when $y_{Pi} \notin I_h$ and $\delta_h(y_{Pi})=0$. Otherwise, $\delta_h(y_{Pi})=1$.

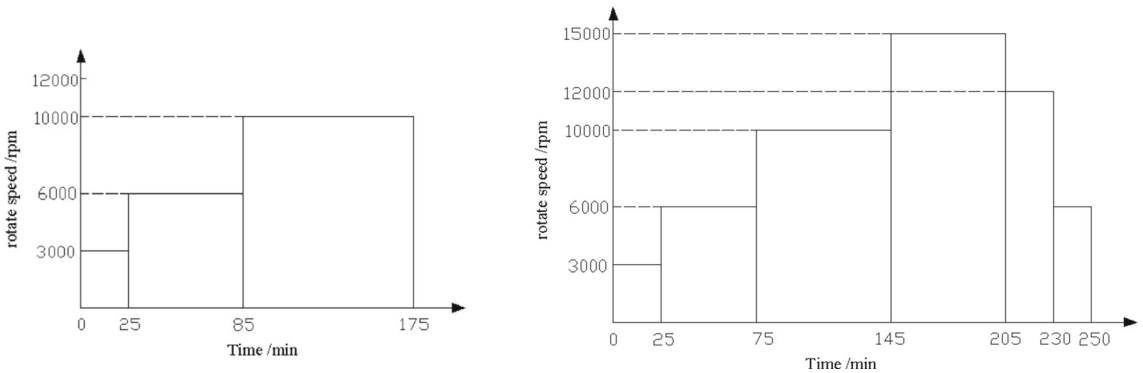

(a) Speed one (b) Speed two

Fig. 4 Spindle speed settings in experiment

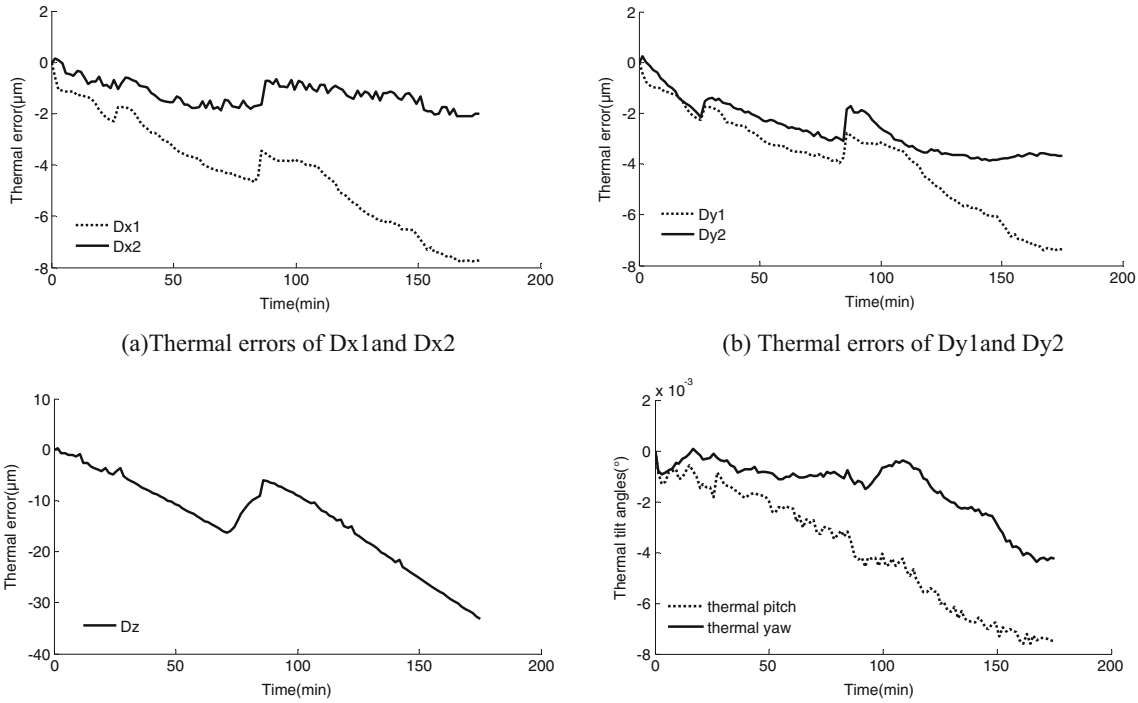

(a)Thermal errors of Dx1and Dx2

(b) Thermal errors of Dy1and Dy2

(c) Thermal errors of Dz

(d) Thermal tilt angles

Fig. 5 Five error curves

Meanwhile, $\tilde{X}$ is sorted in accordance with y_P, and the new temperature sample X_P is sliced into $J_1, J_2, \cdots, J_H$.

③ Mean calculation of sliced sample

After slicing, compute the sample means of $I_1, I_2, \cdots, I_H$ and $J_1, J_2, \cdots, J_H$, respectively, which are expressed as $\overline{l}_1, \overline{l}_2, \cdots \overline{l}_H$ and $\overline{m}_1, \overline{m}_2, \cdots \overline{m}_H$.

④ Principal component analysis on sample mean

Conduct a principal component analysis on the temperature sample means $\overline{m}_1, \overline{m}_2, \cdots \overline{m}_H$ in the following: calculate the weighted covariance matrix $V = \sum_{h=1}^{H} \hat{p}_h \overline{m}_h \overline{m}_h^T$ and find the k largest eigenvectors named as η_r $(r=1,2,\cdots,k)$. Finally, determine the parameter vector $\beta_r = \eta_r \sum_{xx}^{-1/2} (r=1,2,\cdots,k)$.

⑤ Projection calculation

Compute the projection Z in e.d.r space, where $Z=\{[z_1,z_2,\cdots,z_k] | z_i=\beta_i X, 1 \le i \le k\}$.

5 Experimental modeling with SIR

5.1 Experiment setting for data acquisition

The experiments were implemented on a precise horizontal machining center as shown in Fig. 2.

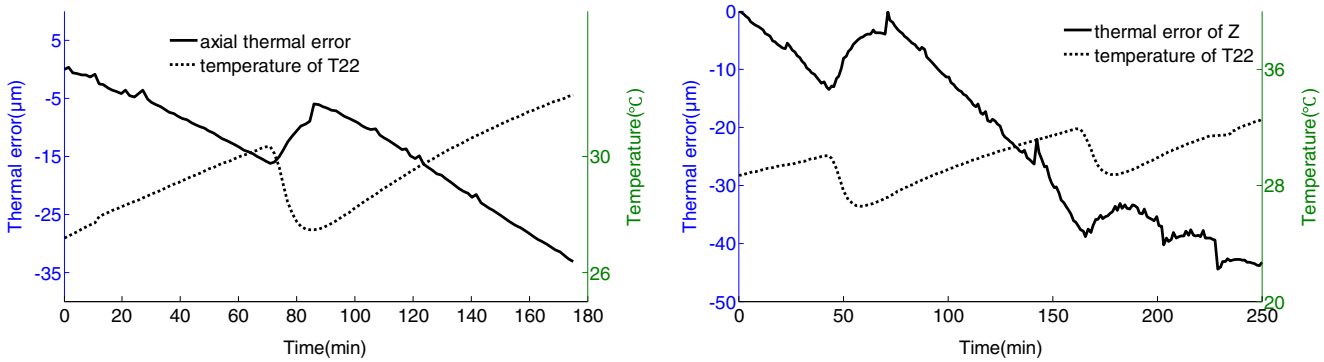

(a) thermal error and temperatureT22 of speed one

(b) thermal error and temperatureT22 of speed two

Fig. 6 Curve of thermal error and cooling fluid temperature

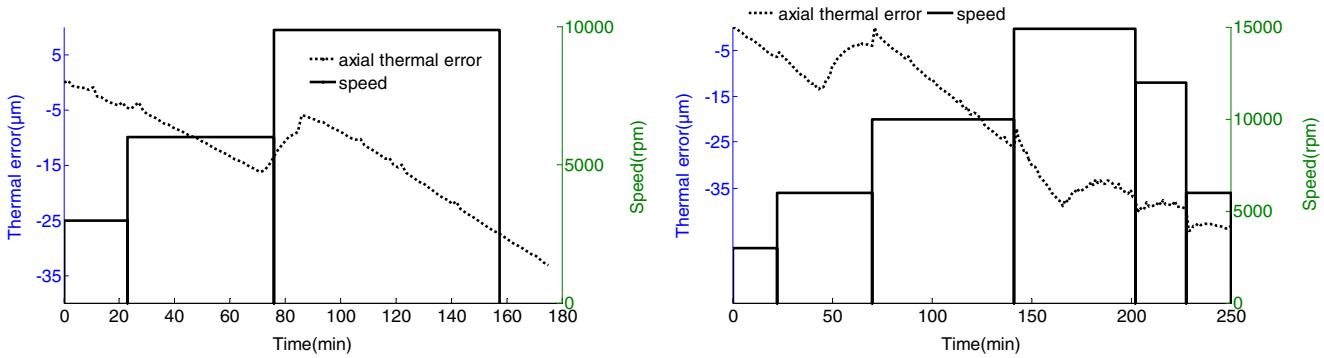

(a) Thermal error and speed one (b) Thermal error and speed two

Fig. 7 Curves of thermal error and speed

Twenty-nine thermocouples were distributed on the machine. Among which, thermocouples T22 and T29 detected the temperature of cooling fluid and environment, respectively. The other thermocouples numbered were dispersed over the machining center as the following:

(1) T4, T6, T21, T23, T24, and T26 on spindle
(2) T16 and T27 on column
(3) T2 on headstock
(4) T1, T8, T9, T12, and T14 on motors and couplings
(5) T5, T7, T15, T19, T20, and T25 on screw nut and screw bearing
(6) T3, T10, T11, T13, T17, and T28 on guide rail
(7) T18 on worktable.

According to ISO 230–3, five displacement sensors were used to detect thermal expansion as shown in Fig. 3. Dx1 and Dx2 detect the thermal error in *X* direction. Dy1 and Dy2 are used to measure the thermal error in *Y* direction. The axial thermal expansion is detected by Dz.

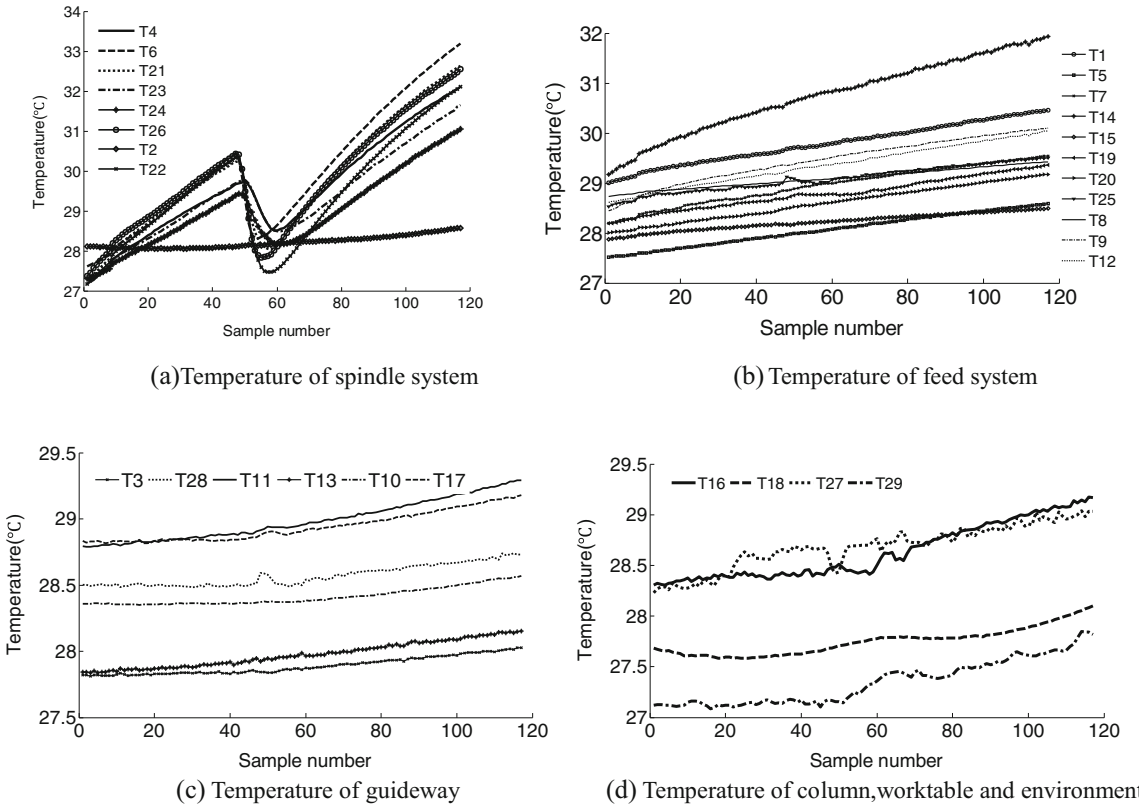

(a)Temperature of spindle system (b) Temperature of feed system

(c) Temperature of guideway (d) Temperature of column,worktable and environment

Fig. 8 Temperature curves

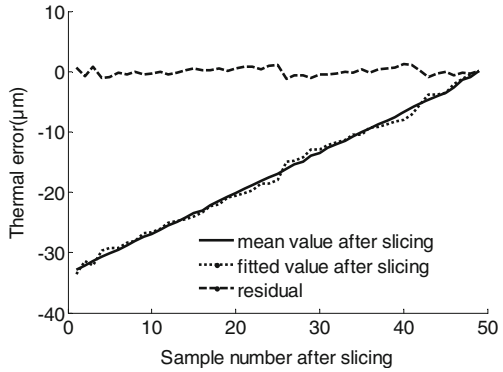

Fig. 9 Fitting results of SIR model

To simulate the machining process in different conditions, feed speed is set as 3000 mm/min and the spindle rotates with two types of speeds as shown in Fig. 4. In experiment, the carriage moves along three directions.

5.2 Data analysis

5.2.1 Analysis of five errors

Under the two speed settings, thermal errors were detected. The data from two experiment conditions show that the axial thermal error is much bigger than the two radial thermal errors. Meanwhile, the radial thermal tilt angles calculated by the data from four radial thermal errors are also small. The five errors under speed one can be seen from Fig. 5. In this paper, the axial thermal error is selected as dependent variable in thermal error modeling.

When the machine was cooled by cooling system, the forced cooling fluid passed through the spindle, which minimized heat generation and thermal expansion. In Fig. 6a, forced cooling starts after the machine worked for 75 min. Thermal error decreases with the decrease of coolant temperature. In Fig. 6b, two major fluctuations of thermal error are corresponding to the twice significant drop of cooling fluid temperature. Moreover, the thermal error fluctuates with the speed variation, which can be seen from Fig. 7.

5.2.2 Analysis of temperature

Under the speed one, the temperature curves of the 29 sensors are shown in Fig. 8. The spindle temperature decreased when the forced cooling fluid passed through the spindle. So, the temperatures of T4, T6, T21, T23, T24, and T26 should be similar with the cooling fluid temperature T22, as can be seen from Fig. 8a. Compared with the seven curves, the fluctuation of headstock is small. In feed system, sensors mounted on motors show high temperature. Thermocouples mounted on the symmetrical position of guideway or column have close temperature curves.

5.3 Modeling of SIR

Based upon the experimental data of speed one, the maximum value of evaluation model is 21.3268, which classifies temperature variables into five groups as

① T1~T3, T5, T7~T17, T19, T20, T25, and T28;
② T4, T6, T21~T24, and T26;
③ T18;
④ T27;
⑤ T29.

Then, five temperature candidates are determined as T18, T19, T24, T27, and T29 based upon the correlation coefficients between temperatures and axial thermal error, although the evaluation model tries to ensure the variable tightness in each group and big distance between temperature groups. Collinearity among temperature candidates cannot be completely avoided. To further eliminate collinearity, SIR introduces principal component analysis.

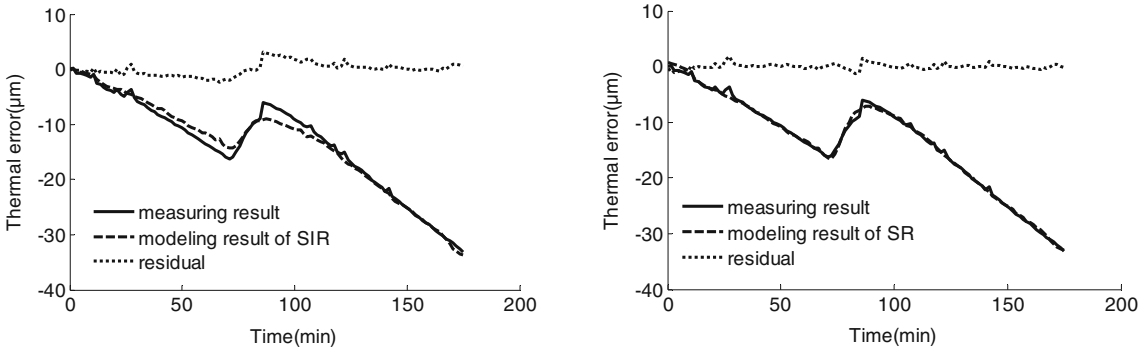

(a) Curve of SIR (b)Curve of SR

Fig. 10 Modeling results of two models

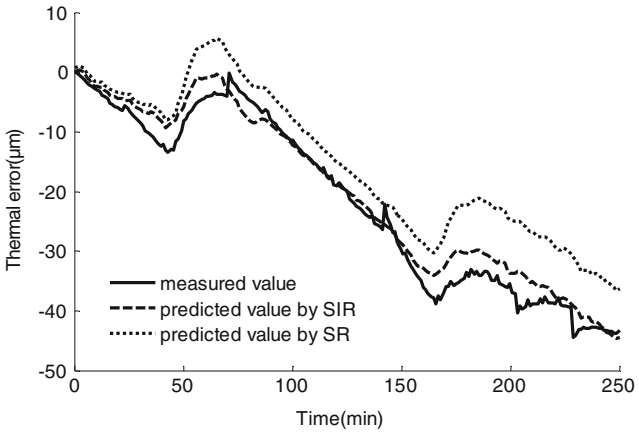

Fig. 11 Prediction results of two models

The temperature increments $\Delta t_{18}, \Delta t_{19}, \Delta t_{24}, \Delta t_{27}, \Delta t_{29}$ between the real-time temperature values and the initial temperature values are used as independent variables. We denote $\Delta t_{18}, \Delta t_{19}, \Delta t_{24}, \Delta t_{27}, \Delta t_{29}$ as t_1, t_2, t_3, t_4, t_5. The axial thermal error is dependent variable represented by z.

In SIR modeling, thermal error and the standardized temperature data are sorted firstly and divided into 49 slices, respectively. After the calculation of sample mean $\overline{m}_1, \overline{m}_2, \cdots \overline{m}_{49}$ and $\overline{l}_1, \overline{l}_2, \cdots \overline{l}_{49}$, a principle component analysis is made on the sample mean $\overline{m}_1, \overline{m}_2, \cdots \overline{m}_{49}$ to eliminate the information overlapping of five temperature candidates T18, T19, T24, T27, and T29. The contributing rates of the first two principal components are 60.408 and 39.104 %. The accumulative contribution is more than 99 %, which proves that the two principal components contain the main information of the five temperature candidates. It is clear that the newfound principle components are unrelated and can successfully eliminate collinearity of five temperature candidates with minimum loss information.

The formulas of the first and the second principal components are

$$Z_1 = 0.1123t_1 + 0.2967t_2 + 0.9081t_3 + 0.2048t_4 + 0.1813t_5 \quad (9)$$

$$Z_2 = 0.6061t_1 + 0.2965t_2 - 0.3616t_3 + 0.3854t_4 + 0.5152t_5 \quad (10)$$

When replacing the five temperature increments t_1, t_2, t_3, t_4, t_5 with two principal components Z_1, Z_2, the five-dimensional model of thermal error can be simplified into two-dimensional model.

With formulas (9) and (10), the projection Z_{t1} and Z_{t2} of the sliced 49 temperature variables on the first and the second principal components are

$$Z_{t1} = [4.0563, 2.2632, \cdots, 0.0139] \quad (11)$$

$$Z_{t2} = [-0.0744, 1.9157 \cdots, 0.0023] \quad (12)$$

In above, the length of Z_{t1} and Z_{t2} is 49.

In thermal error modeling, the data $\overline{l}_1, \overline{l}_2, \cdots \overline{l}_{49}$ are defined as outputs, and the projection Z_{t1} and Z_{t2} are regarded as inputs. Under regression theory, the model is established as

$$z = 0.9639 - 8.4200Z_1 - 7.0439Z_2 \quad (13)$$

The fitting curve of 49 sample means is shown in Fig. 9. Apparently, the fitting accuracy of the 49 data is very high.

5.4 Comparison between SIR model and SR model

(1) Comparison of fitting accuracy

In Sect. 5.3, SIR model is established upon the 49 sample means of speed setting one. Then, all temperature data are projected with formulas (9) and (10). Next, the projection data are put into formula (13). The modeling result is pictured as Fig. 10a. The residual is within 3.1 μm. The determination coefficient is 0.985.

To discuss the performance of SIR model, SR has been applied for temperature variable optimization and thermal error modeling. From three alternative models, the model constructed by $\Delta t_{24}, \Delta t_{27}, \Delta t_{29}$ has the best performance. The axial thermal error z is described as

$$z = 0.7059 - 8.1186t_3 + 1.1345t_4 - 6.0832t_5 \quad (14)$$

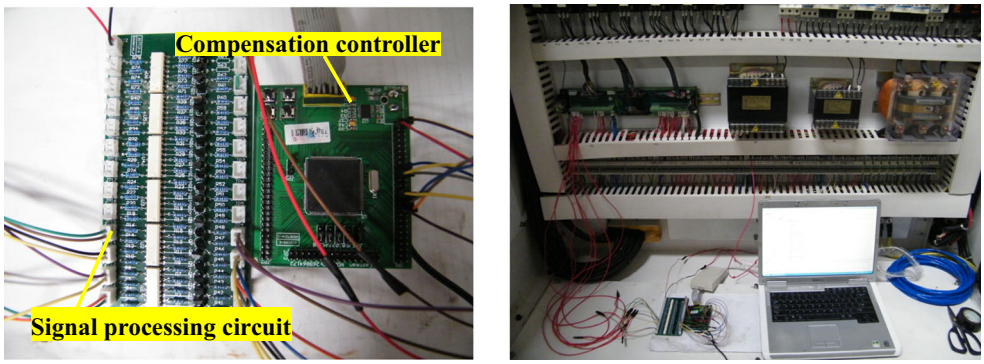

(a) Hardware of compensation system (b) Wiring at experiment site

Fig. 12 Hardware and wiring in compensation experiment

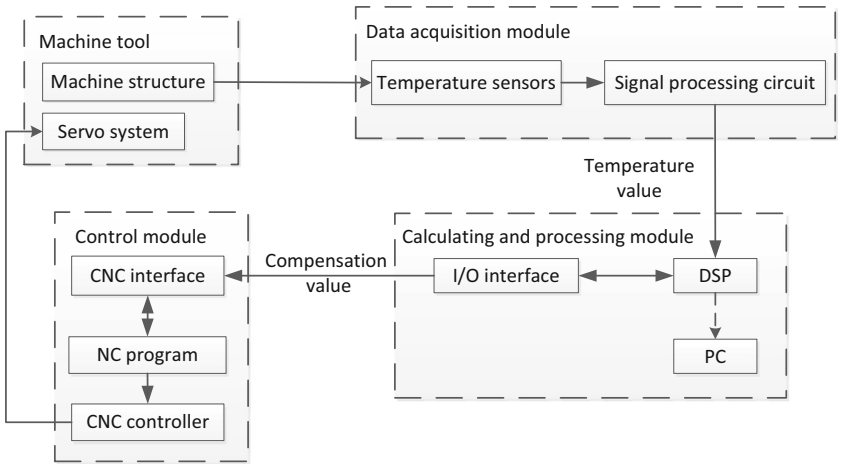

Fig. 13 Block diagram of thermal error compensation

The modeling result is shown in Fig. 10b. The fitting curve is very close to the measured curve. The residual is within 2.5 μm, and the model determination coefficient is 0.991. Since the SR model is built upon all samples of speed one, while the SIR model is established upon 49 mean samples, the accuracy of SR is slightly higher than that of SIR. On the whole, both of the two models have high fitting accuracy.

(2) Prediction accuracy comparison

In thermal error modeling, robustness is an important performance. A model established from on condition might not fit for the compensation in another condition. To verify the effectiveness and robustness of the proposed model, another experiment was performed under the speed two as Fig. 4b. The established two models based upon the data from speed one are used to predict the thermal error of speed two. The verification result is shown in Fig. 11. The predicted value by SIR is closer to the measured value, which proves that the SIR model has good robustness, while the prediction accuracy of the SR model is poor. With the smaller prediction deviation, the SIR model is more suitable for error compensation than the SR model.

6 Thermal error compensation

6.1 Compensation system

To testify the performance of SIR model, a thermal error compensation system was developed. The compensation controller and circuit connection is shown in Fig. 12.

Before compensation, sensors are used to measure temperature and thermal error. Next, a thermal error model is established in PC with measured data and embedded in digital signal processing (DSP). The block diagram of compensation is shown in Fig. 13. The compensation system is composed of three modules as data acquisition module, calculating and processing module, and control module. In thermal error compensation, temperature sensors are firstly place on the key points of machine tool to measure temperatures. Secondly, the temperature signals are processed by signal processing circuit. Then, the processed temperature signals are set to DSP. Next, according to the model embedded in DSP, compensation value is calculated and the correlated controlling signals are sent to CNC controller through circuit interfaces. Finally, the CNC control system compensates the thermal error automatically.

6.2 Performance verification of error compensation

Under speed two, compensation experiment was conducted to evaluate the performance of the SIR model. In the compensation experiment, the axial thermal error was measured in real time. Figure 14 gives the error before and after compensation. It can been seen that the axial thermal error is reduced from 43 μm (without compensation) to 7 μm (with compensation). The SIR model is effective in thermal error compensation.

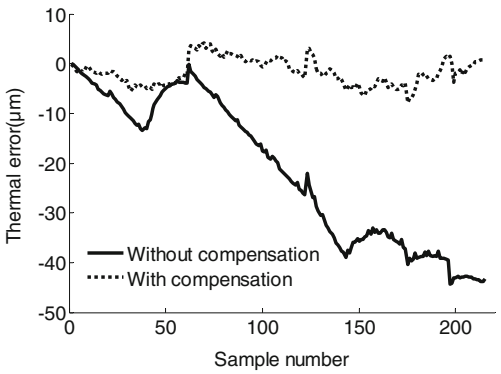

Fig. 14 Comparison of errors with and without compensation

7 Conclusions

This paper proposes a new thermal error model base upon SIR in order to establish the relationship between the thermal error and the temperature. Under the hypothesis of nonlinear model, the methodology can effectively reduce the dimension of input variables without sacrificing variable information. Meanwhile, the model can further eliminate the collinearity between inputs. Before modeling, an evaluation model based upon fuzzy clustering is advanced for temperature classification. Under the maximum evaluation value, an optimal temperature classification can be found. Then, one temperature variable from each group is selected according to its correlation coefficient with thermal error. Through the method, the number of temperature sensors was reduced from 29 to 5. The selected five temperature candidates are used as the inputs of SIR model.

A SR model is also built for thermal error prediction in this paper. Experimental results show that the maximum fitting residual of the two models is less than 3.5 μm and the determination coefficients are both greater than 0.95, which proves the high accuracy of the two models. While in the verification of model effectiveness under speed two, the SIR model has smaller prediction error. Therefore, the SIR model has better robustness than the SR model. A real-time error compensation experiment indicates that the accuracy of a precise horizontal machining center was improved significantly and the axial thermal error was reduced from 43 to 7 μm.

Acknowledgments The authors would like to express their thanks to the funds of Nanjing Institute of Technology (Number CKJB201401) and the Special Foundation of the Central University Basic Business (3082014NS2014045).

References

1. Pahk HJ, Lee SW (2002) Thermal error measurement and real time compensation system for the CNC machine tools incorporating the spindle thermal error and the feed axis thermal error. Int J Adv Manuf Technol 20(7):487–494
2. Abdulshahed AM, Longstaff AP, Fletcher S (2015) The application of ANFIS prediction models for thermal error compensation on CNC machine tools. Appl Soft Comput 27:158–168
3. Mian NS, Fletcher S, Longstaff AP, Myers A (2013) Efficient estimation by FEA of machine tool distortion due to environmental temperature perturbations. Precis Eng 37:372–379
4. Mayr J, Ess M, Weikert S, Wegener K (2009) Compensation of thermal effects on machine tools using a FDEM simulation approach. Proceedings of the 9the LAMDAMAP 38–47.
5. Wu CW, Tang CH, Chang CF, Shiao YS (2012) Thermal error compensation method for machine center. Int J Adv Manuf Technol 59:681–689
6. Han J, Wang LP, Wang HT (2012) A new thermal error modeling method for CNC machine tools. Int J Adv Manuf Technol 62:205–212
7. Vyroubal J (2012) Compensation of machine tool thermal deformation in spindle axis direction based on decomposition method. Precis Eng 36(1):121–127
8. Chen JS, Yuan J (1996) Thermal error modelling for real-time error compensation. Int J Adv Manuf Technol 12:266–275
9. Li Y, Yang J, Zhang H, Tong H (2006) Application of grey system model to thermal error modeling on machine tools, Knowledge Enterprise: Intelligent Strategies in Product Design, Manufacturing, and Management, Springer, 511-518
10. Yao XH, Fu JZ, Chen ZC (2008) Bayesian networks modeling for thermal error of numerical control machine tools [J]. J Zhejiang Univ Sci A 9(11):1524–1530
11. Lee JH, Lee JH, Yang SH (2001) Thermal error modeling of a horizontal machining center using fuzzy logic strategy. J Manuf Process 3(2):120–127
12. Ramesh R, Mannan MA, Poo AN (2002) Support vector machine model for classification of thermal error in machine tools. Int J Adv Manuf Technol 20:114–120
13. Miao EM, Gong YY, Niu PC, Ji CZ, Chen HD (2013) Robustness of thermal error compensation modeling models of CNC machine tools. Int J Adv Manuf Technol 69:2593–2603
14. Wu H, Yang JG, Zhang HT (2008) Synthetically modeling for the thermal error and cutting force induced error on a CNC turning center. J Sichuan Univ (Eng Sci Ed) 40(2):165–169
15. Guo QJ, Yang JG, Wu H (2010) Application of ACO-BPN to thermal error modeling of NC machine tool. Int J Adv Manuf Technol 50:667–675
16. Wu H, Yang JG, Zhang HT, Wang XS (2008) Thermal error robust modeling and real time compensation on CNC turning center. J Shanghai Jiao Tong Univ 2(7):1064–1067
17. Ramesh R, Mannan MA, Poo AN (2003) Thermal error measurement and modeling in machine tools. Part II: hybrid Bayesian network-support vector machine model. Int J Mach Tool Manuf 43:405–419
18. Zhang Y, Yang JG, Jiang H (2012) Machine tool thermal error modeling and prediction by grey neural network. Int J Adv Manuf Technol 59:1065–1072
19. Li Y, Zhao WH, Lan SH, Ni J, Wu WW, Lu BH (2015) A review on spindle thermal error compensation in machine tools. Int J Mach Tool Manuf 95:20–38
20. Zhao HT, Yang JG, Shen JH (2007) Simulation of thermal behavior of a CNC machine tool spindle. Int J Mach Tool Manuf 47(2): 1003–1010
21. Han J, Wang L, Wang H, Cheng N (2012) A new thermal error modeling method for CNC machine tools. Int J Adv Manuf Technol 62:205–212
22. Yan JY, Yang JG (2009) Application of synthetic grey correlation theory on thermal point optimization for machine tool thermal error compensation. Int J Adv Manuf Technol 43:1124–1132
23. Zhang T, Ye WH, Liang RJ, Lou PH, Yang XL (2013) Temperature variable optimization for precision machine tool thermal error compensation on optimal threshold. Chin J Mech Eng 26(1):158–165
24. Ker-Chau L (1991) Sliced inverse regression for dimension reduction. J Am Stat Assoc 86(414):316–327